

THE EFFECT OF FREQUENCY AND WAVE SHAPE GENERATED BY A SYNTHETIC JET ACTUATION ON THE COOLING OF MICROCHIPS WITH CHANNELS FILLED WITH WATER

D. Li, V. Timchenko, J.A. Reizes, E. Leonardi

School of Mechanical and Manufacturing Engineering, The University of New South Wales,
Sydney 2052, Australia.

Abstract

Since the heat generated by a microchip is directly proportional to the operating frequency squared and to the circuit density, improvements in microchip performance require significant enhancements in thermal management. Micro-channels with synthetic jet cooling devices have been shown to be an effective approach in lowering the maximum chip temperature. In order to optimize the heat transfer between the silicon substrate and cooling fluid, parameters such as, the diaphragm amplitude, frequency and jet velocity wave shape have been varied. Cases with frequencies of 280, 560 and 1120 Hz have been investigated. The results indicate that with the same jet Reynolds number, the temperature in the silicon decreases with frequency. There is no increase in the heat transfer rate when the expulsion time is shortened and the suction time is lengthened while keeping the cycle period constant.

Introduction

Increased power dissipation as the result of increased frequency of operation and circuit density, as well as shrinking device size of the integrated electronic circuits, have placed extreme performance requirement on the thermal management of microelectronic components. The present methods of temperature control, such as the use of ever larger heat sinks is plainly inadequate when dealing with heat fluxes of the order of 1 MWm^{-2} , or greater, so that active modes of cooling need to be considered. Synthetic jets actuators, consisting of a cavity with a moving diaphragm and an orifice in the face opposite the diaphragm, have been suggested as cooling enhancing devices. The oscillation of the diaphragm results in an alternating entrainment and ejection of fluid through the orifice and the forming of a series of vortex rings in the channel. Unlike traditional jets, there is zero net mass flux into or out of the cavity even though there is a net positive momentum transferred into the region outside the cavity [5]. Because such actuators do not require complex plumbing, they appear to be particularly well suited for enhancing heat transfer from microchips.

Two possible methods of using synthetic jets to increase heat transfer rates have been explored; these being impinging jets in an otherwise quiescent flow and impinging jets into a cross flow. A number of experimental studies have been performed which focused on the impingement of synthetic jets on surfaces in a quiescent flow. The near field was observed with different driving elements and configurations. Trávníček *et al.* [9] investigated the influence of diaphragm amplitude and frequencies on the air jet characteristics. The authors indicated that large amplitudes lead to the quick break-up of vortices formed as the result of separation at the exit from the orifice. On the other hand, when small amplitude was used vortices retained their shape further downstream. Furthermore, at high excitation frequencies the vortices broke up into small scale eddies while at low frequencies, the large vortices impinge onto the heated surface.

Pavlova *et al.* [4] studied the effect of frequencies and orifice to surface distance ratio on heat transfer. They showed that high frequency (1200Hz) jets yield higher heat transfer rates when the H/d ratio (H is the distance between the heated surface and the orifice and d is the orifice diameter) is between 5-12, whilst at low frequency (420Hz) better performance is achieved than at high frequency when the $H/d > 16$. They also demonstrated that heat transfer decreases considerably when $H/d > 20$ at both frequencies and maximum heat transfer seems to occur at the ratio of 5-10.

In general agreement with Pavlova *et al.* [4], Kercher *et al.* [2] found an optimum H/d ratio in the range of 6.3-8.4 for synthetic jets using air when the actuator operated at its resonance frequency. However, in a more recent experimental study Gillespie *et al.* [1], demonstrated that although the maximum local heat transfer coefficient occurs at $H/d=7$, the average Nusselt number reaches its maximum at $14 < H/d < 18$. Moreover, the authors suggested that the cavity temperature is a function of H/d with the internal cavity temperature rising to a peak value when $10 < H/d < 20$.

Unfortunately, the cooling rates obtained with synthetic jets operating in a quiescent flow did not generate sufficiently high heat transfer fluxes. Similarly, since the present techniques of cooling heat sinks with airflow from fans are reaching the limits of their capabilities, alternate methods such as those employing synthetic jets into a cross flow, are now also being considered. Milanovic *et al.* [3], derived a correlation equation for jet penetration and jet-to-cross-stream momentum ratio. They found that there was a lower jet penetration at high cross-flow velocities and that the penetration of the synthetic jet is proportional to the jet velocity at the orifice.

Much of the experimental research on synthetic jets, used macro-scale equipment and therefore the resulting data might not be applicable to micro scale devices. Micro scale devices have been studied numerically by Timchenko and her co-workers in both an open atmosphere and in a micro-channel with a constant pressure difference between channel's ends [6, 7]. The configuration studied consisted of a micro-channel etched in the rear side of the silicon chip and the synthetic jet actuator, is shown in Figure 1. Air and water have been used as the cooling medium with a channel Reynolds number around 100 and an average jet Reynolds number around 130. It was shown that when air is used there is an increase in the heat flux, and it is a function of the frequency used. Regrettably, forced convection using air, even in combination with synthetic jets to enhance heat transfer of the laminar flow is not sufficient for cooling microelectronic components in the 1 MWm^{-2} heat flux range [7]. However when water was used, both the minimum and maximum temperature in the silicon wafer were significantly reduced.

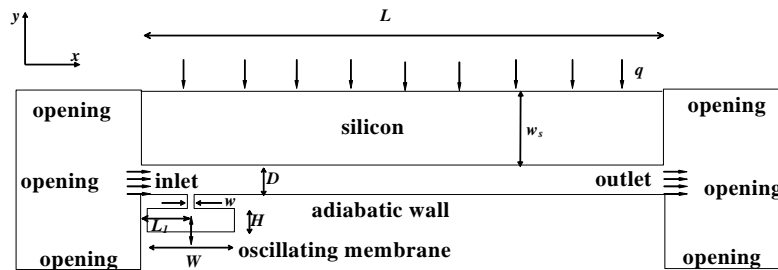


Figure 1. Sketch of the computational domain.

Because of the long run times necessary to obtain reliable quasi-steady data, only one flow arrangement was studied by Timchenko *et al.* [8]. It is at present not known what the effect of different flow ratios, diaphragm frequencies and the driving signal wave shapes, is on the heat transfer from a silicon wafer. This paper is therefore aimed at answering these questions.

Mathematical and Numerical Models

Mathematical Model

The two-dimensional computational model has been developed by Timchenko *et al.* [8] and is re-used here. A channel with a height of $200 \mu\text{m}$, and length of 4.05 mm , is etched at the rear side of the silicon and opened at either end, with big headers. Water enters the inlet header marked opening on the left of Figure 1, and passes through the channel, finally leaving the computational domain through the outlet marked opening on the right side of Figure 1. The inlet and outlet of the computational domain should be treated as openings since flow comes in and goes out from the boundary at the same time. The left and right side of the silicon are cooled by water in the headers.

A synthetic jet actuator is attached to the lower wall of the channel, with an orifice and a cavity. The orifice has a width of $50 \mu\text{m}$, and height of $100 \mu\text{m}$, which is located 1.1 mm downstream of the channel entrance. The width of the diaphragm is 2 mm , and the cavity height is $400 \mu\text{m}$.

Instantaneous temperature distributions in silicon and the fluid as well as velocity fields in the channel were calculated by using the commercial package, ANSYS CFX 11. Water has been used as the working fluid in the micro-channel and has been assumed to be an incompressible fluid. The fluid flow affected by the periodic motion of the synthetic jet and by the constant pressure difference between the channel ends, was simulated by using the three conservation equations, namely: conservation of mass,

$$\nabla \cdot \tilde{V} = 0 ; \quad (1)$$

conservation of momentum, the Navier-Stokes equation,

$$\rho_l \frac{\partial \tilde{V}}{\partial t} + \rho_l \nabla \cdot (\tilde{V} \tilde{V}) = -\nabla p + \mu \nabla^2 \tilde{V} \quad (2)$$

and conservation of energy,

$$\rho_l \frac{\partial h_l}{\partial t} + \rho_l \nabla \cdot (\tilde{V} h_l) - k_l \nabla^2 T_l = 0, \quad (3)$$

in which, $\rho, \tilde{V}, p, \mu, h, T, k$ and t denote density, the velocity vector, the gauge pressure, dynamic viscosity, enthalpy, absolute temperature, thermal conductivity and time. The subscript l refers to the liquid.

The temperature distribution in the silicon was solved using the Fourier Equation, viz,

$$\rho_s \frac{\partial h_s}{\partial t} = k_s \nabla^2 T_s \quad (4)$$

in which the subscript s refers to the solid.

The coupling between the fluid and solid domain obtain by matching the instantaneous heat flux at the interface, viz,

$$k_l \left(\frac{\partial T_l}{\partial n} \right)_i = -k_s \left(\frac{\partial T_s}{\partial n} \right)_i, \quad (5)$$

in which n refers to the outward drawn normal and the subscript i indicates an interface.

The cavity temperature varies with the periodic motion of the synthetic jets, and an increase of the cavity temperature has been observed in our previous research [8]. As a result, the flow in the actuator is fully simulated. The displacement of the diaphragm which is assumed to be a parabola varies sinusoidally in time, viz,

$$Y_m = A \left(1 - \left(\frac{2x}{W} \right)^2 \right) \sin(2\pi ft) \quad (6)$$

in which A is the maximum centerline amplitude, f is the frequency of membrane oscillation and W is the width of the diaphragm. It should be noted that the period of oscillation, τ of the diaphragm is $\tau = 1/f$.

In this work, it is proposed to simulate a non-sinusoidal variation in time, of the membrane driving signal wave shape. For example if the expulsion time is reduced to about $2/3$ of the original expulsion duration and the ingestion time is increased to $4/3$ of the original ingestion duration, thereby having the same over all τ , equation (6) becomes,

$$Y_e = A \left(1 - \left(\frac{x}{W} \right)^2 \right) \cos(3\pi ft + n\pi), \quad (7)$$

for the ejection part of the cycle and

$$Y_s = A \left(1 - \left(\frac{x}{W} \right)^2 \right) \sin\left(\frac{3}{2}\pi ft + \frac{1}{2}n\pi\right), \quad (8)$$

for the ingestion phase. The subscripts e and s refer to expulsion and the suction phase respectively and n refers to the cycle number. An internal function in CFX was used for switching between the two equations. However, as there are 200 iterations in one cycle, and a time step at $1/3$ of the iterations appears not to be an integer number which makes the monitoring of the crucial time step impossible when expulsion and suction phases are

switching, a slight change was made to the equations. In order to monitor the phase switching, while still approximately retaining the expulsion time at 2/3 of the original expulsion duration, equations (7) and (8) were rewritten as:

$$Y_e = A(1 - (\frac{x}{W})^2) \cos(\frac{20}{7} \pi ft + \frac{8}{7} n\pi), \quad (9)$$

for the ejection part of the cycle and

$$Y_s = A(1 - (\frac{x}{W})^2) \sin(\frac{40}{27} \pi ft + \frac{14}{27} n\pi), \quad (10)$$

for the ingestion phase. Since a full simulation of the diaphragm motion was undertaken, it was necessary for the mesh to distort in the vicinity of moving membrane.

Numerical Method

Second order backward Euler differencing in time, and a second order upwind differencing in space were used for discretizing equations (1 - 3). A second order upwind differencing scheme was chosen to save a computational time as a central differencing would require reducing of time step and discrepancy between results obtained using these two schemes was insignificant. 200 time steps were used per cycle and the internal iterations of each time step were continued until the mass, momentum and energy residuals had been reduced to 2×10^{-5} . In [8], the internal residuals at each time step have been reduced to 10^{-7} . However, the results obtained when the residuals were only 2×10^{-5} , had differences of less than 0.5% for heat flux, 0.05% for velocity and 0.003% and temperature respectively, so that the limit of 2×10^{-5} was used here to stop iterations, thus saving considerable CPU time.

The same mesh as that used by Timchenko *et al.* [8] is used here. This consists of 50×20 grid points in the stream-wise and transverse direction respectively in the orifice of the actuator so that the mesh size in the orifice is $2.5 \mu\text{m}$ square. The grid then gradually expands to a maximum mesh size of $5 \mu\text{m}$ outside the orifice. The total number of mesh points employed was 261,154.

Boundary Conditions

A constant heat flux of 1 MWm^{-2} , was applied to the top surface of the silicon wafer and all other walls were set adiabatic. Water entered with a temperature of 20°C through the opening on the left hand side. A constant pressure difference of 750 Pa was set between inlet and outlet. 280 Hz , 560 Hz and 1120 Hz were used as frequencies for driving the diaphragm. Different jet Reynolds numbers were obtained by varying the amplitude of the diaphragm.

Results and Discussion

The channel Reynolds number is defined as $Re_c = \rho \bar{u}_c D / \mu_l$, \bar{u}_c is the average axial channel cross sectional velocity, given by $\bar{u}_c = (1/\tau D) \int_t^{t+\tau} \int_0^D u(X, y, t) dy dt$, $u(X, y, t)$ is the instantaneous axial velocity, X is any location along the channel.

The jet Reynolds number is defined as $Re_o = \rho_l \bar{v}_0 w / \mu_l$, in which $\bar{v}_0 = 2/\tau w \int_{t_0}^{t_0+\tau/2} \int_{-w/2}^{w/2} v(x, 0, t) dx dt$ is the average ejection velocity through the orifice, $v(x, y, t)$ the instantaneous vertical velocity and t_0 the time when ejection starts.

The discussion which follows is divided into two sections. The effects of, the actuator driving frequency and the type of actuation (that is, whether it is sinusoidal or not), on the heat

transfer rates from the silicon wafer and the temperature distributions in both computational domains are discussed first. Then the effects of the actuator frequency and actuation type on the fluid flow are used to interpret the heat transfer and temperature distribution results.

Heat Transfer: Sinusoidal Diaphragm Excitation

As mentioned above, all results presented when a sinusoidal excitation is used, that is equation (6) was employed to represent the diaphragm motion, have boundary conditions with a pressure difference of 750 Pa between the ends of the channel and a Reynolds number at the orifice of approximately 130.

When the actuator was not activated, the channel Reynolds number Re_c resulting from the pressure difference between the ends of the channel was about 100. The jet Reynolds number was kept at 130 when varying the membrane oscillating frequency and amplitude. The transient simulations when the synthetic jet was activated were started from the steady state result where only the pressure difference was acting.

Temperature contours in the silicon wafer, when a frequency of 560 Hz was used to drive the diaphragm, are presented in Figure 2. As can be seen from the figure the maximum temperature occurs at the top of silicon near the channel outlet while the minimum temperature, as may have been expected happens on the lower part of the silicon just near the channel entrance.

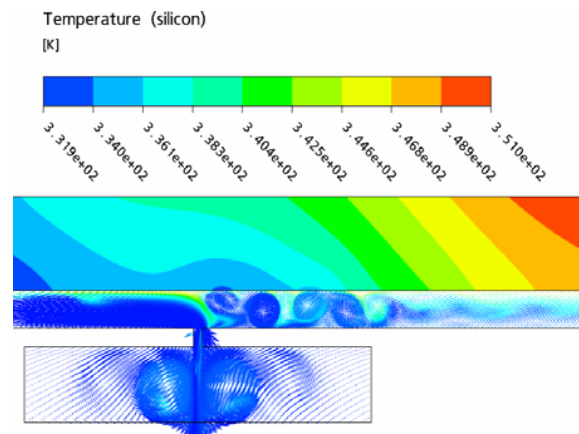


Figure 2. Temperature contours in the silicon and vortical structure of flow in the channel at the time of maximum ingestion velocity; operating frequency is 560 Hz .

The complex vortical structure at the time of maximum ingestion is also shown in Figure 2, in which the velocity vectors are coloured by the temperature. It is clear that the flow is well mixed near the orifice of the actuator. However, the vortical activity is significantly reduced about 1 mm downstream from the orifice. One of the difficulties in using synthetic jets is that the actuator may take in fluid which is already hot, however as may be seen in Figure 2 even at the point of maximum ingestion only cold fluid enters the cavity. This cold fluid is ejected and "strikes" the hot wall thereby causing the vortical motion and significantly increasing the heat transfer rate as is indicated in Figure 3, by the fact that all temperatures fall from their steady flow values when the actuator is switched on.

Numerical simulations were also performed at 280 Hz , and 1120 Hz , with the same jet Reynolds number as was used at 560 Hz . The effect of varying the driving frequency is shown in Figure 3 for the first 0.08 s after starting the actuator. This is a sufficiently long enough time to determine whether the performance is improved by using frequencies other than 560 Hz , since results for this frequency have been already published in

[8].

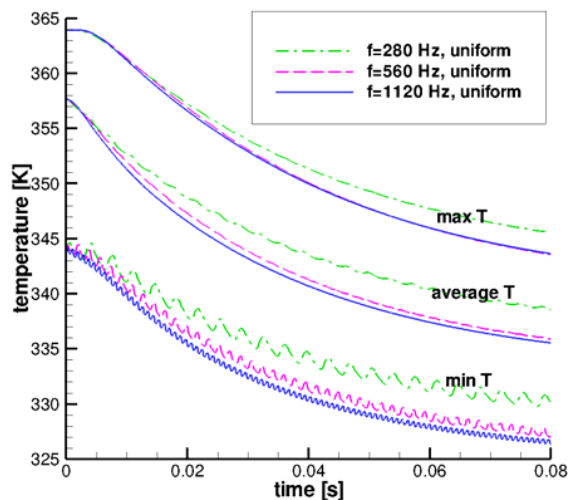


Figure 3 Temperature distributions in silicon for sinusoidal actuation. Dash dot line $f=280\text{ Hz}$; dash line $f=560\text{ Hz}$; solid line $f=1120\text{ Hz}$.

The transients of the maximum temperature in the silicon for the three cases are indicated by the upper curves in Figure 3. There is very little change in this transient between the diaphragm being driven at 560 Hz or 1120 Hz . However, at the end of the calculation period the maximum temperature of the silicon is about 2°C higher when the driving frequency is reduced to 280 Hz .

The largest change from the steady flow case is in the minimum silicon temperature which occurs on the face in contact with the cooling water as may be seen in Figure 2 and represented by the lower curves in Figure 3. There are significant variations, with the temperature drop increasing as the driving frequency is increased. Whereas after 0.06 s there is less than 1°C between the cases when 560 and 1120 Hz are used, the minimum temperature is 3.5°C hotter when the diaphragm is driven at 280 Hz rather than at 1120 Hz .

The differences between the transients in the average temperature of the silicon wafer as a function of driving frequency are given by the middle curves in Figure 3. As may have been expected, differences between these temperatures as a function of actuator driving frequency, fall between the differences in the maximum and minimum temperatures.

It is interesting to note that in Figure 3 the minimum temperature is affected by the periodic nature of the synthetic jet flow, as is demonstrated by a periodic variation in time of that temperature. The amplitude of the periodic variations is inversely proportional to the frequency, whereas the frequency of the periodic temperature is perforce equal to the driving frequency of the diaphragm. However, due to the thermal inertia of the wafer, the only periodic variation in the average temperature of the wafer occurs at the very lowest frequency and there is no discernable periodic variation in time of the maximum temperature.

It can be seen in Figure 4 that the average heat flux on the lower surface of the silicon wafer also fluctuates cyclically. Since the periodic flow induced by the synthetic jet actuator, causes these fluctuations in the heat flux, their frequency is the same as the frequency of the diaphragm oscillations. Since the silicon wafer has thermal inertia, it follows that the longer fluid action takes, the larger the effect. The amplitude of the

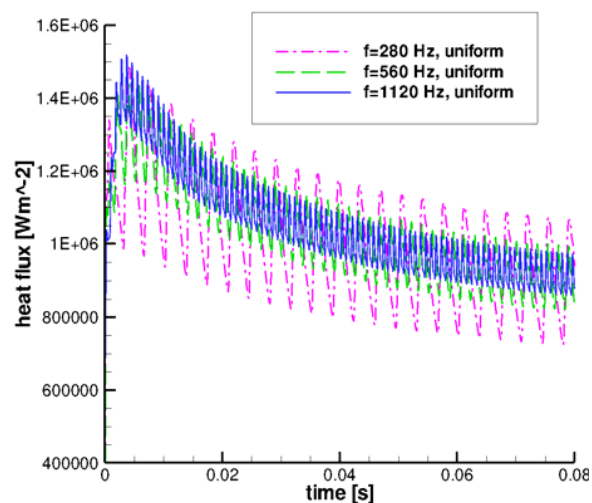


Figure 4 Heat flux at the silicon and flow interface for sinusoidal actuation. Dash dot line $f=280\text{ Hz}$; dash line $f=560\text{ Hz}$; solid line $f=1120\text{ Hz}$.

heat flux fluctuations is therefore inversely proportional to the frequency which is consistent with the temperature oscillations in the minimum temperature shown in figure 3.

Although differences in the amplitude of the heat flux are significant, differences in the average heat flux during a whole cycle, as may be seen in Table 1, are much smaller. Here and for all results shown in the following tables, the data have been averaged for one cycle and in all cases the averaging was started at 0.0357 s when the suction phase began. It should be remembered that there is heat transfer on the right and left sides of the silicon wafer in contact with cooling water, so the area for heat removal from the wafer is larger than the area through which it is heated on the top. At all times the total heat removed from the wafer was in fact greater than the heat input of 1 MWm^{-2} through the top which leads to the microchip itself being cooled below the temperatures which occurred in steady flow before switching the actuator on.

The differences in the average heat flux on the lower surface of the silicon wafer account for the maximum, average and minimum temperatures in the silicon being noticeably higher when the actuator is driven at 280 Hz than at the other two frequencies. Since the heat fluxes at 560 and 1120 Hz differ by less than 0.5% (rounding of the figures in Table 1 exaggerates the difference), the temperature in the silicon wafer are much the same at these two frequencies.

Driving frequency	280 Hz	560 Hz	1120 Hz
Cycle averaged heat flux	993 kWm^{-2}	1027 kWm^{-2}	1029 kWm^{-2}
Amplitude variation	378 kWm^{-2}	202 kWm^{-2}	131 kWm^{-2}

Table 1. Cycle averaged heat flux for sinusoidal actuation.

One of the difficulties in using synthetic jets for heat transfer enhancement is that during the ingestion period some of the already heated fluid might be taken in to the cavity. It follows that the average temperature of the fluid as it enters the cavity is a very important parameter to monitor directly, since it affects the ejection and average cavity temperature. Values of the

Driving frequency	280 Hz	560 Hz	1120 Hz
Ingestion averaged temperature	295.24 K	294.97 K	295.55 K
Expulsion averaged temperature	294.55 K	294.28 K	295.44 K
Cycle averaged temperature	294.93 K	294.70 K	295.50 K
Amplitude of temperature variation	9.75 K	10.90 K	7.39K

Table 2. Averaged temperature at the orifice for sinusoidal actuation.

temperatures of the fluid leaving and entering the orifice averaged over parts of the actuator cycle are shown in Table 2 for the cycle starting at 0.0357s. It can be seen that for actuator driving frequencies of 280 and 560 Hz, the differences in the mean temperatures of the water entering the cavity and the temperatures of the fluid leaving the cavity are about the same.

The fact that the temperature of the water ejected from the cavity is less than the temperature of the ingested fluid is due to the fact that “quasi-equilibrium” has not yet been reached when the temperatures of the water entering and leaving the cavity would be equal. When the actuator is operated at 1120 Hz, there have been four times and twice as many diaphragm cycles respectively than when 280 and 560 Hz are used as the driving frequencies. It follows that in the same time from starting the actuator there has been much more opportunity for mixing of the water entering the cavity with the water in the cavity. As a consequence temperature of the water leaving the cavity is much closer to that entering it at 1120 Hz.

Before starting the actuator, the velocity and temperature distributions were steady. With the pressure difference of 750 Pa applied between the ends of the calculation region, a laminar flow resulted with the temperature of the fluid near the hot silicon surface increasing as the fluid moved downstream. Because the flow was laminar, there was no mixing, so that the thermal boundary layer was very thin with the temperature of the major part of the flow remaining at 293K. Since the temperature of the water ingested by the actuator is greater than 293K, as is clear from Table 2, some already heated water is then taken into the cavity. If the ingestion period were increased as a proportion of the overall cycle period while taking the same quantity of water, as was done in the case of sinusoidal excitation, the temperature of the ingested water should be less and the average heat flux greater at the interface between the silicon and water.

Heat Transfer: Non-sinusoidal Diaphragm Excitation

In this case equations (9) and (10) were used to represent the diaphragm motion. As a consequence of the longer suction phase of the cycle, the expulsion phase has to be shorter since the same overall period is to be used. It follows that if the same volume of water has to be expelled, but in a shorter time, the velocity through the orifice has to increase, as may be seen in Table 3. This leads to a significantly larger Reynolds number than in the case of the equivalent sinusoidal excitation. When the non-sinusoidal excitation mode is used, the average expulsion velocity becomes equal to 3.36 m/s instead of 2.36 m/s for uniform excitation and therefore the Re number becomes 187 instead of 130 when a sinusoidal excitation is employed.

Driving frequency	280 Hz	560 Hz	1120 Hz
Ingestion averaged temperature	296.58 K	295.92 K	297.07 K
Expulsion averaged Temperature	295.73 K	295.52 K	296.95 K
Cycle averaged temperature	296.35 K	295.84 K	297.11 K
Amplitude of temperature variation	12.54 K	11.88 K	8.56 K

Table 3. Averaged temperature at orifice for nonsinusoidal actuation.

Average temperatures at the exit of the orifice for non-sinusoidal actuation are presented in Table 3. As may be seen by comparing the values in Table 2, despite the increased time that the water is ingested into the cavity, the fluid temperature at the orifice during this phase increased. The exact opposite of what had been postulated! Therefore, surprisingly, as may be seen by comparing the values in Table 1 with those in Table 4, the heat flux is increased when a driving frequency of 280 Hz is used, it remains at approximately the same at 560 Hz whereas it is reduced at 1120 Hz relative to the values when a sinusoidal excitation is used.

Driving frequency	280Hz	560Hz	1120Hz
Cycle averaged heat flux	1017kWm ⁻²	1032kWm ⁻²	979kWm ⁻²
Amplitude of variation	538 kWm ⁻²	251 kWm ⁻²	149kWm ⁻²

Table 4. Cycle averaged heat flux for nonsinusoidal actuation.

As the consequence of the increased heat transfer rate at 280 Hz, the difference between the temperatures when 560 Hz is used and when 280 Hz is employed are significantly reduced as may be seen by comparing figures 3 with figure 5. In sharp contrast, the temperature differences between using 1120 Hz and 560 Hz have significantly increased. In any case since the heat flux at 560 Hz has not changed, the use of the complex driving function given by equations (9) and (10) does not seem to be beneficial.

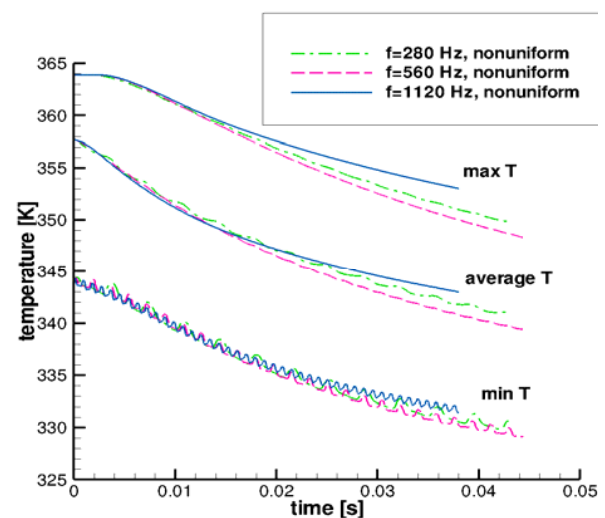


Figure 5 Temperature distributions in silicon for nonsinusoidal actuation. Dash dot line f=280 Hz; dash line f=560 Hz; solid line f=1120 Hz.

Further, since the temperature in the cavity will eventually equilibrate with the inlet fluid temperature, the fact that the orifice temperature has been increased will eventually lead to higher fluid temperatures during the discharge phase, thereby reducing the heat transfer rate, so that any additional study of the non-sinusoidal driving function was abandoned.

These unexpected results can only be explained by examining the flow patterns which occur when different operating conditions are modelled.

Flow Fields: Sinusoidal Diaphragm Excitation

The flow fields generated with a sinusoidal excitation are discussed first, followed by the flow fields obtained when the diaphragm is activated by a non-sinusoidal signal.

Unlike a jet operating in an otherwise stationary fluid, no vortex train is formed during the expulsion phase of the actuator cycle as may be seen in figure 6 in which the computed instantaneous velocity vectors are shown at different instants in the cycle beginning at 0.0357s for the frequency of 1120Hz. The velocity vectors in Figure 6(a), occur at a time that the diaphragm is moving at its maximum velocity towards the orifice. By this stage the expelled water from the the orifice has reached the upper wall of the channel thereby interfering with the boundary layer in the region in which heat transfer occurs. The emerging jet from the orifice generated the clockwise vortex immediately down stream of the jet and at the same time it generated a small anticlockwise vortex near the upper surface on the downstream side of the jet.

Since the flow is two-dimensional, as may be seen in Figure 6(a), when the jet impinges on the upper surface, the flow in the main channel is separated into two parts with no flow from the region upstream of the dividing jet to that down stream. This leads to a complete flow reversal in the area upstream of the jet so that a complex flow pattern begins to develop, caused by the interaction of the flow reversal and the developing vortex. Downstream of the impinging jet the motion is sustained by the jet and the remnant of the vortices from the previous cycle.

As may be seen in Figure 6(b), at the end of expulsion stage the impinging jet is “reflected” from the upper surface thereby strengthening the clockwise vortex generated by the jet emerging from the orifice on the downstream side of the orifice and forming a counter-clockwise vortex on the downstream side of the first reflection from the upper wall. This new, counter clockwise vortex is strengthened by the reflection of the jet from the lower side. This is repeated a number of times so that a series of geared vortices are created which are separated by the main flow from the jet.

Further, during the suction phase, as may be seen in Figures 6(c) and 6(d) most of the fluid enters the cavity rather than continuing along the main channel, so that there is a significantly reduction in velocity in the main channel during the suction phase of the actuator cycle. Velocities averaged over the inlet and outlet areas are shown as functions of time in figure 7. The amplitude of the inlet velocity fluctuations is significantly larger than those at the outlet. Since the actuator is nearer the inlet than the outlet any pressure increase or decrease will have a larger effect on the shorter channel, so it is expected that the velocity oscillations should have a larger effect on the inlet than the outlet.

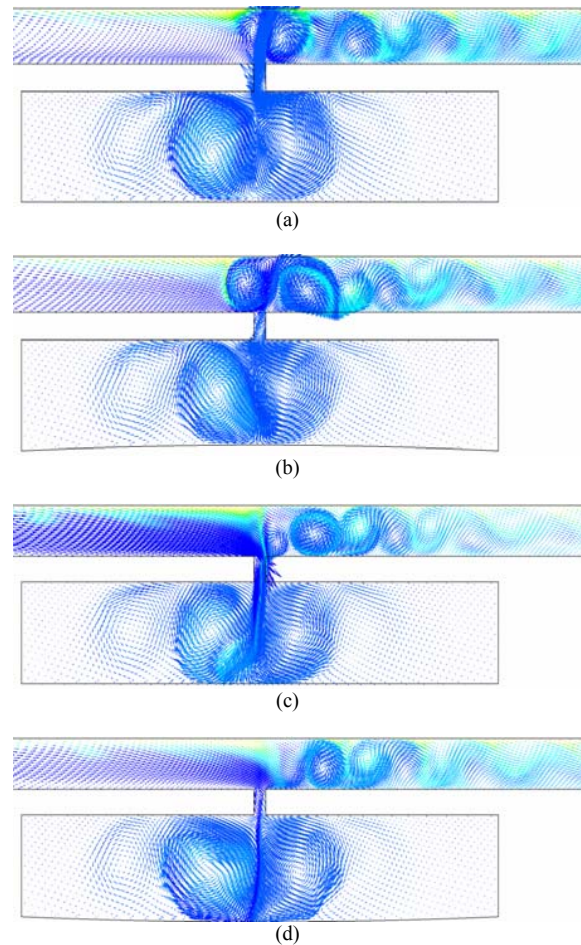


Figure 6. Vortical structure in microchannel.

It should be noted in figure 7 that there is a net outflow through the entrance to the channel during part of the ejection phase of the actuator cycle. However, there is no net inflow at any stage through the outlet. The inlet and outlet velocities averaged over space and one diaphragm cycle as may be seen in Table 5, less than the steady state velocity of 0.49 m/s because of the blockage over part of the cycle by the jet of the main channel.

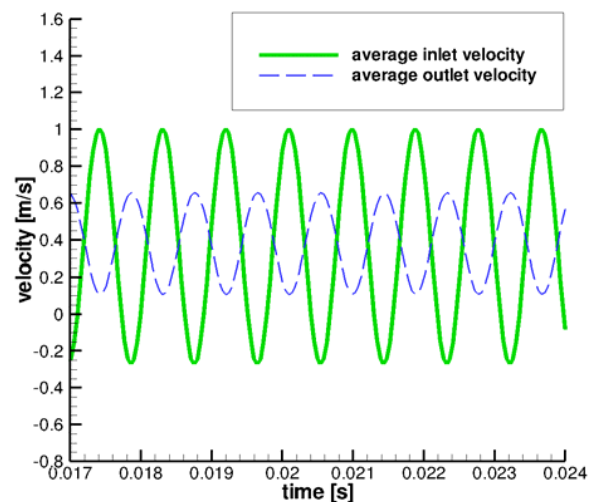


Figure 7. Average velocity at channel inlet and outlet, $f=1120\text{ Hz}$, sinusoidal actuation. Dash line outlet velocity; solid line inlet velocity.

	Inlet velocity	Outlet velocity
Ingestion average velocity	0.741 m/s	0.231 m/s
Expulsion average velocity	0.00582. m/s	0.545 m/s
Cycle average velocity	0.373 m/s	0.389 m/s
Amplitude of variation	1.280 m/s	0.549 m/s

Table 5. Average velocity at channel outlet, $f=1120\text{ Hz}$, sinusoidal actuation.

The flow reversal and the fact that there are vortices upstream of the orifice are clear indications that there is some mixing upstream of the orifice. This is the reason for the temperature during the suction part of the cycle not being equal to the cold water temperature at the inlet to the calculation region.

When the frequency of the diaphragm is reduced to 560 and 280 Hz respectively, with the average exit velocity from the orifice over time and space maintained at the same value, the structure of the flow and the vortices at the same phase of the cycle relative to the jet velocity at the exit of the orifice passage, remains the same and need not be discussed any further. What changes is the number of vortices upstream and downstream of the orifice. And this affects the average velocity through the channel so that at $f=280\text{ Hz}$, the inlet average velocity for a whole cycle is 0.405 m/s and outlet average velocity is 0.420 m/s. For 560 Hz the inlet and outlet velocities through the cycle are 0.440 m/s and 0.457 m/s respectively. These values are larger comparing with average inlet and outlet velocity for $f=1120\text{ Hz}$ (see Table 5) which indicates the maximum blockage of the flow exists at 1120 Hz.

During the suction stage the geared vortices persist, but is weakened as time progresses, while the axial velocity is reduced as may be seen in Figures 6(c) and 6(d). What is not clear in Figure 6(c) is that the vortex which was upstream of the orifice in Figure 6(b) has moved to be just downstream of the orifice. Similarly, the other vortices, shown in Figure 6(b) have moved downstream with significant loss of strength. The vortices continue to move downstream during the remainder of the suction phase as may be seen in Figure 6(d).

The clockwise rotating vortices increase the velocity near the hot wall and quickly remove the hot fluid from the neighbourhood of the hot wall while bring cool fluid from the deeper part of the channel, thereby significantly increasing the rate of heat transfer. The fact that the vortices are geared means that when the rotation is anti-clockwise, fluid velocity is reduced and indeed sometimes reversed in the vicinity of the hot silicon wafer. This slow moving hot fluid reduces heat transfer, whilst the rate of conveying fluid from the cooler parts of the channel is also reduced. As may be seen in figure 6, the vortex action is significantly reduced, about 2mm downstream of the orifice, from which point there is little or no enhancement. In fact, because the fluid, when the actuator is used is hotter than in the steady flow case, there can be reductions in heat transfer below the steady state values, further downstream than 2mm from the orifice. The net result, as discussed above, is a significant increase in heat transfer, which might be able to be optimised by either a better placement of the orifice, using more than one actuator or perhaps changing the type of actuation from a sinusoidal signal to another type, for example that given by equations (9) and (10).

Flow Fields: Non-sinusoidal Diaphragm Excitation

As mentioned above when the non-sinusoidal excitation mode is used, Re becomes 187 rather than 130 when a sinusoidal excitation is employed. This strongly affects both inlet and outlet velocities in the channel as can be seen in Figure 8 for $f=1120\text{ Hz}$. Outflow through the entrance to the channel during part of the ejection is stronger with a maximum velocity for the reversed flow at the entrance of -0.6 m/s comparing to -0.2 m/s for uniform case. For the outlet, the effect is less pronounced but there is still decrease in average velocity to 0.308 m/s comparing with 0.389 m/s for uniform case.

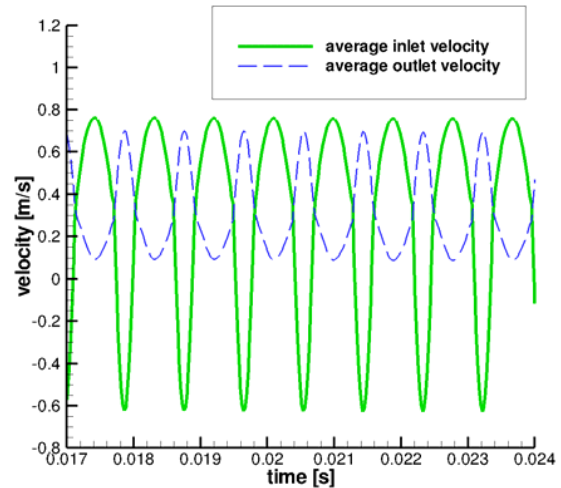


Figure 8. Average velocity at channel inlet and outlet, $f=1120\text{ Hz}$, nonsinusoidal actuation. Dash line outlet velocity; solid line inlet velocity.

The same behaviour applies for $f=280\text{ Hz}$ and $f=560\text{ Hz}$ where the increase in Re number and therefore strength of jet flow strongly affects the inlet of the channel and also leads to reduction of the average velocity through the channel.

Conclusion

The effects of frequency and jet wave shape of a synthetic jet on the heat transfer and fluid structure has been investigated using a two-dimensional numerical model. Frequencies of 280, 560 and 1120 Hz were employed with the same jet Reynolds number for the sinusoidal excitation cases. The temperature in the silicon varies with frequencies and the largest effect of frequency occurs in the minimum silicon temperature. The lowest minimum temperature in silicon occurs at 560 Hz, while the lowest maximum temperature is similar for both frequencies at 1120 Hz and 560 Hz. When the jet Reynolds number is increased by shortening the expulsion time, the temperature in silicon is further reduced for 280 Hz and 560 Hz compared with uniform phase cases.

References

- [1] Gillespie, M.B., Black W.Z., Rinehart.C., & Glezer, A, Local Convective Heat Transfer From a Constant Heat Flux Flat Plate Cooled by Synthetic Air Jets, *Transaction of the ASME*, Vol.128, October 2006.
- [2] Kercher, D.S., Lee, J.B., Brand, O., Allen, M.G, Member, IEEE, & Gleze, A., Microjet Cooling Devices for Thermal Management of Electronics, *IEEE*, Vol 26, No.2, June 2003.
- [3] Milanovic, I.M. & Zaman, K.B.M.Q, Synthetic Jet in Crossflow, *AIAA journal*, Vol 43, No.5, May 2005.
- [4] Pavlova, A. & Amitay, M., Electronic Cooling Using Synthetic Jet Impingement, *Journal of heat transfer*, Vol.128, September 2006, 897-907.

16th Australasian Fluid Mechanics Conference
Crown Plaza, Gold Coast, Australia
2-7 December 2007

- [5] Smith, B.L. & Glezer, A., The Formation and Evolution of Synthetic Jets, *Phys.Fluid* **10**, 1998, 2281-2297.
- [6] Timchenko, V., Reizes, J., Leonardi, E and G. de Vahl Davis, A Criterion for the Formation of Micro Synthetic Jets, *2004 IMECE*, Anaheim, CA USA, November 13-19, 2004.
- [7] Timchenko, V., Reizes, J. & Leonardi, E., An Evaluation of Synthetic Jets for Heat Transfer Enhancement in Air Cooled Micro-channels, *Int. J. Numerical methods for Heat & Fluid Flow*, Vol. **17**, No. 3, 2007.
- [8] Timchenko, V., Reizes, J., Leonardi, E. and Stella, F., Synthetic Jet Forced Convection Heat Transfer Enhancement in Micro-Channels, *Proceedings 13th International Heat Transfer Conference*, Begell House Inc., New York, Published on CD-Rom, ISBN: 1-56700-226-9, Paper MIC-21, 2006
- [9] Trávníček, Z. & Tesař, V., Annular Synthetic Jet Used for Impinging Flow Mass-Transfer, *International journal of heat and mass transfer* **46**, 2003, 3291-3297.